Letter

Controlling Blend Morphology for Ultra-High Current Density in Non-Fullerene Acceptor Based Organic Solar Cells

xin Song, Nicola Gasparini, Long Ye, Huifeng Yao, Jianhui Hou, Harald Ade, and Derya Baran

ACS Energy Lett., **Just Accepted Manuscript** • DOI: 10.1021/acsenergylett.7b01266 • Publication Date (Web): 23 Jan 2018

Just Accepted

ACS Energy Letters is published by the American Chemical Society. 1155 Sixteenth Street N.W., Washington, DC 20036

Controlling Blend Morphology for Ultra-High Current Density in Non-Fullerene Acceptor Based Organic Solar Cells

Xin Song, Nicola Gasparini, Long Ye, Huifeng Yao, Jianhui Hou, Harald Ade*, Derya Baran**

X. Song, Dr. N. Gasparini, Prof. D. Baran

Division of Physical Sciences and Engineering, KAUST Solar Center (KSC), King Abdullah University of Science and Technology (KAUST), Thuwal, Saudi Arabia

Dr. L. Ye, Prof. H. Ade

Department of Physics, Organic and Carbon Electronics Lab (ORaCEL), North Carolina State University, Raleigh, NC 27695, USA

Dr. H. Yao, Prof. J. Hou

State Key Laboratory of Polymer Physics and Chemistry, Beijing National Laboratory for Molecular Sciences, Institute of Chemistry, Chinese Academy of Sciences

Beijing 100190, P. R. China

Corresponding author email: hjhzlz@iccas.ac.cn , hwade@ncsu.edu, derya.baran@kaust.edu.sa

Abstract:

In this report, we highlight a system with a well-known polymer donor (PTB7-Th) blended with a narrow bandgap non-fullerene acceptor (IEICO-4F) as active layer and 1-chloronaphthalene (CN) as the solvent additive. The optimization of the photoactive layer nanomorphology yields short-circuit current density value of 27.3 mA/cm^2, one of the highest value in organic solar cells reported to date, which competes with other types of solution processed solar cells such as perovskite or quantum dot devices. Along with decent open-circuit voltage (0.71V) and fill factor values (66%), a power conversion efficiency of 12.8% is achieved for the champion devices. Morphology characterizations elucidate that the origin of this high photocurrent is mainly due to increased π-π coherence length of the acceptor, the domain spacing as well as the mean-square composition variation of the blend. Optoelectronic measurements confirm a balanced hole and electron mobility and reduced trap-assisted recombination for the best devices.

TOC

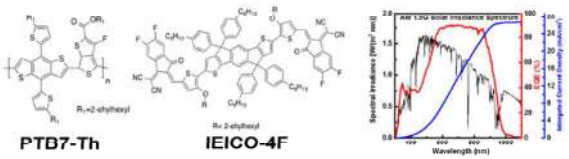

High photo-current density (J_{sc}) along with high open-circuit voltages (V_{oc}) is a sine-qua-non for champion efficiency organic solar cells (OSC). In the case of OSCs, band gap engineering can be utilized to lower the band gap of materials (usually donor) for efficient photon harvesting and higher J_{sc}; however, some of the achievable V_{oc} would be lost in the meantime due to decreased effective energy gap between donor and acceptor (usually fullerene derivative, i.e. $PC_{61}BM$ or $PC_{71}BM$).[1–8] For example, diketopyrrolopyrolle (DPP) derivatives possessed remarkably high J_{sc} but suffered from low V_{oc} due to low lying lowest unoccupied molecular orbital (LUMO) of fullerene derivatives.[9–11] The low absorption profile of $PC_{61}BM$ or $PC_{71}BM$ in the visible and near-infrared (NIR) region also limited the photon capture ability of these devices.[12–15] In the last decade, the urge for fullerene replacements for higher V_{oc} whilst maintaining high J_{sc} has been of significant interest to synthesis groups in the field of OSCs.[16,17] Recently, small molecule non-fullerene acceptors (NFA) emerged as superior alternatives to fullerene derivatives.[18,19] These materials provide strong absorption coefficient along with energy level tunability that can maximize the V_{oc} and J_{sc} when low band gap derivatives are used to harvest photons matching the solar flux in NIR region.[20,21]

Recent report shows that the J_{sc} obtained in NFA-based OSCs can reach values over 25 mA/cm^2 (Figure 1a, the photocurrent values as a function of band gap for photovoltaics and SQ limit), which is comparable with other state-of-the-art technologies (perovskites, quantum dots).[22–26] However, low *FF* of these devices limit the PCE to 10% (see Table S1, supporting information). Amorphous or less-crystalline high efficiency donor polymers such as PTB7-Th allows rapid polaron conversion and intermixed nano-morphology but the devices suffer from the *FF* for thick active layers which is necessary for scale-up procedures.[12,20] Therefore, these devices are optimized for ~100nm thick active layer which is not optimal for roll-to-roll applications and

thick active layers using these donors would be desirable. Controlling the nano-morphology by improving the face-on orientation in the active layer and reduced recombination losses would improve the photo-to-current conversion along with *FF*.[28,29] Combining with device engineering, the performance can be improved to close the gap to SQ limit, which would further bring OPVs competitive with other solution processable photovoltaic solar cells.[30,31]

In this work, we report an ultra-high photo-current along with a decent FF obtained from a medium band gap polymer donor PTB7-Th and a low band gap NFA (IEICO-4F) system by controlling the morphology evaluation with solvent additive treatment. In the optimal conditions (4% 1-chloronaphthalene (CN) v/v), we achieve a current density of up to 27.3 mA/cm^2 (26.5 mA/cm^2 average) and a PCE of 12.8% without further post-annealing treatment or interfacial modifications. We determine that a sufficient amount of CN plays a crucial role to simultaneously increase the face-on orientation, NFA crystallization and coherence length as demonstrated by grazing incidence wide-angle X-ray scattering (GIWAXS), as well as improving the average domain purity as shown with R-SoXS, thus contributing to the improvement of J_{sc} and FF. Besides, we elucidate the origin of high photocurrent by understanding the photo-physics of the champion devices varying the amount of CN. We conclude that PTB7-Th:IEICO-4F devices with 4% CN exhibit lower trap-assisted recombination and balanced hole/electron mobility, leading to one of the highest photo-current polymer:NFA solar cell devices reported so far.

The chemical structures of PTB7-Th and IEICO-4F are shown in Figure 1b. Normalized absorbance spectra and absorption coefficient of neat films are shown in Figure 1c and Figure S1, respectively. As previously reported,[20] IEICO-4F is an ultra-narrow bandgap NFA material with an absorption window in the range from 600 nm to 1000 nm. In order to obtain reproducible

device performance and stability,[32] we utilize inverted device configuration (ITO/ZnO(~35 nm)/Active layer(~150 nm)/MoO_x(~5 nm)/Ag(~100 nm)) with a fixed donor:acceptor ratio (1:1.5, w:w) and host solvent (CB). All parameters of energy levels in the device configuration are obtained from the literature (shown in Figure 1d).[16,20] Figure 2a and Table 1 describe the current density (*J*)- voltage (V) curves and photovoltaic parameters of PTB7-Th:IEICO-4F devices under 100 mW/cm^2 light illumination. Interestingly, the addition of 4% CN improves J_{sc} from 23.7 mA/cm^2 to 27.3 mA/cm^2 and FF from 53.6% to 65.6%. The improvement of these two parameters pushes the PCE from 9.23% to 12.8%, an enhancement of 38.7%. However, further addition of CN (7% v/v) decreases the current density (24.5 mA/cm^2), whilst maintaining the FF. In addition, we obtain a PCE of 12.1% with a thickness ~200 nm, which is promising for roll-to-roll or sheet-to-sheet coating processing for commercial applications. In order to ensure the reproducibility of the device results, we constructed more than 40 cells and made the corresponding current density distribution histogram, with an average J_{sc} of 26.5 mA/cm^2 (Figure 2b). More details about the device optimization as a function of CN amount and active layer thickness are shown in Figure S2 to S4. The details of the performance parameters and standard deviations are also provided in Table S2 to S4. To further confirm the J_{sc} values, we carry out external quantum efficiency (EQE) measurements. As shown in Figure 2c, all EQE curves have a broad wavelength response (ranging from 400 nm to 1000 nm). Notably, the calculated J_{sc} values integrated from EQE data is less than 5% mismatch as compared to the values extracted from the *J*-V characteristics. In detail, 0% CN devices exhibit EQE values lower than 80% between 600-900 nm, while flat EQE curve with values up to 90% in the same region is presented in 4% CN cells. In contrast, 7% CN devices show lower EQE values in comparison with that of 4% CN devices, especially in the range of 700 nm to 900 nm (corresponding to IEICO-4F), suggesting

that an excessive amount of CN has a negative effect on the current generation. The high EQE values obtained for 4% CN devices should lead to an internal quantum efficiency close to unity. Thus, we performed ellipsometry measurements to calculate the n, k values of PTB7-Th:IEICO-4F blend (Figure S4e). According to the method proposed by McGehee group,[27] we calculated for this blend an internal quantum efficiency (IQE) of over 90% in the range of 600 nm to 850 nm (Figure S4f), suggesting an efficient photon-to-charge carriers conversion and carriers collection at the electrodes for 4% CN devices.

Photoluminescence (PL) quenching is also an excellent complementary tool to infer details about exciton dissociation which is often correlated to J_{sc}.[33] The PL quenching of PTB7-Th in PTB7-Th:IEICO-4F blends (Figure S5) shows interesting trends when excited at 682 nm and the results are summarized in Table 1. Notably, the emission peak of pure PTB7-Th (centered at 775 nm) is quenched by 87% and upon addition of IEICO-4F suggesting efficient exciton dissociation in the blend. The PL quenching yield increases up to 96% until 4% CN based blends suggesting an optimal morphology for efficient photoinduced charge transfer and thus a higher J_{sc} of the corresponding devices. However, higher loading of CN (7%) lead to 87% exciton quenching for the PTB7-Th emission peak compared to 4% CN blend, which is due to reduced exciton dissociation in this blend, contributing to yielding slightly lower J_{sc} in the 7% CN devices compared to 4% CN cells.

In general, the ability to convert light into current is often related to the absorption strength of the active layer.[34–36] Thus, we investigate the absorption coefficient of PTB7-Th:IEICO-4F active layers with different CN ratio (Figure 2d). Although the donor:acceptor weight ratio is kept at 1:1.5 in the film without CN, the peak coefficient ratio between the donor and the acceptor without CN is less than 1 (Table S5) because of the different absorption coefficients of PTB7-Th

and IEICO-4F (Figure S1).[16] On the contrary, the peak ratios of blends with 1% CN and 4% CN are greater than and near 1, respectively, which is attributed to the NFA aggregation (discuss later in the GIWAXS part). This tendency is consistent with the increase in EQE between 700-900 nm. It is worth mentioning that blend films with 4% CN depict the highest absorption coefficient with a balanced contribution from donor and acceptor materials, which is in agreement with the highest J_{sc} and EQE values.

To check the impact of CN on the molecular packing and texture, we characterize the PTB7-Th:IEICO-4F films by 2-dimensional grazing incidence wide X-ray scattering (GIWAXS).[37,38] 2D GIWAXS patterns and 1D out-of-plane (OOP) and in-plan (IP) line-cuts of pristine PTB7-Th and IEICO-4F films are illustrated in Figure S6. For the polymer:NFA blends, the 2D GIWAXS patterns (**Figure 3**a-d) and pole figures (Figure 3f), exhibit a preferable face-on orientation ascribed to the strong (010) reflection of π-π stacking in the OOP direction (Figure 3e) observed for all samples.[39] The IP line-cuts of these blend films are depicted in Figure S7. Overall, the absence of strong higher order (h00) peaks indicates paracrystalline disorder and a low degree of crystallinity. The coherence lengths (CL) calculated from the full-width at half maximum (FWHM) of OOP π-π stacking peaks (Figure 3e) via Scherrer equation are summarized in Table 2. With the addition of CN, modest changes of the CL in polymers are observed. Whereas, in the acceptor IEICO-4F part, the CL significantly changes from 2.8 nm to 4.0 nm when CN is introduced, indicating that CN mainly affects the molecular aggregation of IEICO-4F, with the highest impact for 1% CN loading, which is consistent with the absorption spectra and atomic force microscopy (Supporting Information, Figure S8). From our solubility test, the NFA solubility limit is about 25 mg/ml and PTB7-Th is nearly 10 mg/ml in CN solvent, respectively. Furthermore, the boiling point of CB is nearly 120 ^{o}C, which is significantly lower that of CN

(~269 °C).[31] It is reported in literature that the addition of high boiling point additives (such as CN) increase the molecular packing of both the donor and acceptor molecules. [36] We believe that the different drying speed of the mixed solvent with high boiling point additive and different donor and acceptor solubility are the driving force for such increased CL. Additionally, the face-on to edge-on ratios (Figure 3g) can be extracted from pole figures of the (100) peak.[40] Our results indicate 4% CN blends show a face-on to edge-on ratio of ~4.3, which is much higher than other three blends (~3.7). Quantification of OOP π-π stacking intensity via the integration of NFA peak yields a similar trend, and the highest intensity is achieved in 4% CN films, indicating a more ordered packing of NFA. Face-on orientation is widely observed in high-performance organic solar cells and considered as a favorable texture for intermolecular charge transport. It is thus not surprising that the best J_{sc} of the 4% CN devices corresponds to the highest face on/edge on ratio.

To understand the mesoscale morphology of these blends, we employ resonant soft X-ray scattering (R-SoXS) to compare their compositional domain characteristics following our previously established protocols.[41] The R-SoXS profiles (Figure 3h) are acquired at the resonant energy (~283 eV) to get high scattering contrast for these NFA blends.[42] By increasing the CN amount, the long period (center-to-center domain spacing) slightly increases from 30.0 nm, 31.4 nm and 33.0 nm, with 1%, 4% and 7% CN, respectively. We note the q-range of our R-SoXS data is not wide enough to detect all the length scales, however, it will likely not affect the trend of our analysis as the high-q peaks (10-50 nm) are more closely related to the device performance compared to the low-q peaks.[29] The integrated scattering intensity (ISI), a measure proportional to the mean-square variations (i.e. variance) of the composition, is widely used to quantify the relative average domain purity across samples. Higher ISI indicates purer domain

and is often associated with reduced bimolecular recombination.[43] The ISI of the 4% CN film is set to 1 as a reference (see Table 2), and the relative ISI for 0% CN, 1% CN and 4% CN are measured as 0.50, 0.63, 1.00, respectively, in good agreement with increased FF.[2] On the contrary, an excess amount of CN (7%) reduces the relative ISI to 0.59. It is worth noting that a closer inspection of the R-SoXS profile for 7% CN reveals a second peak located at ca. 0.1 nm^{-1} absent from the other devices, which corresponds to a much larger spacing of ~60 nm. This larger length of phase separation may belong to a liquid-liquid phase separation, which is due to the slower drying process in the 7% CN film.[42] Despite lower scattering intensity for 7% CN film, the PTB7-Th:IEICO-4F devices exhibit decent fill factor values (65%) likely due in part to the balanced charge carrier mobility of this device system (Table 1), which still allows efficient charge extraction.[44] We will discuss further details of this special case below.

One common method to elucidate recombination is to investigate the *J-V* characteristics under different light intensity (P). The relationship between J_{sc} and P can be described as $J_{sc} \propto P^{\alpha}$, where α represents a power-law exponent. A linear relationship indicates a negligible effect of bimolecular recombination to the extracted current, whereas, $\alpha<1$ suggests that bimolecular recombination become a limiting factor to the device performance. As shown in Figure 4a, the α values of 0%, 1%, 4% and 7% CN cells, are determined to be 0.971, 0.975, 0.986 and 0.973, respectively, showing that the addition of CN suppresses bimolecular recombination initially, which then improves J_{sc} and FF. Again, the trend is broken between the 4% and 7% devices. Moreover, the dependency of V_{oc} vs P gives information about trap state formation. In particular, by following theoretical considerations, V_{oc} linearly depends on the light intensity with a slope of nkT/q ($1<n<2$), where k is Boltzmann's constant, q is elementary charge, n is scaling factor, and

T is Kelvin temperature.[45] Trap-assisted recombination is identified with a strong dependence of V_{oc} on light intensity with a slope of 2 kT/q (at 300 K) [45], while a slope of kT/q is a signature of purely bimolecular recombination or surface recombination.[47] From Figure 4b, it is clear that the devices with 4% CN have the lowest trap-assisted recombination (1.42 kT/q). Further increasing the amount of CN to 7% causes stronger trap-assisted recombination (1.60 kT/q), due to the lower domain purity compared to 4% CN based devices.[48]

To better understand the charge transport as a function of solvent additive, we measure hole/electron mobility by space charge limited current (SCLC) method.[49] As shown in Figure 4c, Table 1 and Figure S9, the values of hole and electron mobilities are enhanced with increasing the CN content in the blend (hole: 9.35×10^{-5} $cm^2V^{-1}s^{-1}$ to 1.56×10^{-4} $cm^2V^{-1}s^{-1}$ electron: 4.56×10^{-5} $cm^2V^{-1}s^{-1}$ to 1.72×10^{-4} $cm^2V^{-1}s^{-1}$, respectively). This is partly due to the more ordered molecule packing, which can assist the charge transport in the D/A networks. It is reported in literature that unbalanced μ_e/μ_h ratio (more than an order of magnitude) can affect the FF values.[50] In our case, there is an improvement in the both hole and electron mobilities upon CN addition (Figure 4c) but not much difference in the μ_e/μ_h was observable which is not the sole reason for improved FF values in solar cell devices.

To make a deeper investigation of the origin of reduced V_{oc} after the addition of CN, we calculate the charge-carrier density (n) using charge extraction (CE) technique.[51] Figure 4d depicts the measured average n as a function of V_{oc}. It is apparent that, at equivalent charge densities (shaded region), corresponding to 1 sun irradiation, pristine devices show the highest V_{oc}. The addition of 1%, 4% and 7% CN blends exhibit 20 mV, 34 mV and 30 mV lower open-circuit voltages compared to pristine devices, respectively. As reported earlier by Holliday *et al.*,

this reduced V_{oc} can be explained by the more ordered microstructure (confirmed by GIWAXS measurements) and reduced electronic bandgap in the BHJ blends.

Many of the measurements performed showed a distinct break in the trends once the CN concentration was increased from 4% to 7%: The PTB7-Th PL quenching showed maximum quenching at 4%, the R-SoXS exhibited maximum purity at 4% and a more complex two-length scale morphology for 7%, bimolecular recombination was minimized at 4%, packing (coherence length, face-on texture) was optimized at 4%. Not all of these observations are readily understood within a paradigm of a uniform 3D morphology. The relative composition variations do not correlate completely with FF across all devices. We note though that the edge-on/face-on orientation populations including the large disordered fractions not observable with WAXS would change the R-SoXS materials contrast, [52,53] necessitating a complex analysis and normalization that we did not perform and that is, along with details about the morphology formation kinetics, outside the scope of this initial report. Furthermore, vertical stratification can occur, which would lower the scattering intensity, but might aid FF. [54] Neither of these possible subtleties of the morphologies are central to the main observations and achievements presented.

In conclusion, we achieved ultra-high photocurrent of 27 mA/cm^2 in PTB7-Th:IEICO-4F blend, by fine-tuning the active layer morphology, which is comparable with competing photovoltaic technologies based on perovskites and quantum dots. The optimal dosage of CN (4%, v/v) yields larger π-π coherence length and face-on/edge-on ratio. Optical and electronic measurements confirm the increased charge transport and reduced recombination for optimal devices with 4% CN additive which then result in 12.8%. A high performance of 12% is achieved with active layer thicknesses close to 200 nm which is very unusual and unique with an amorphous polymer PTB7-Th. We envision that designing novel ultra-low band gap materials with controlled

molecule packing, nanomorphology and charge recombination is a promising route for future OPV applications with high efficiencies.

Acknowledgements

D. Baran acknowledges KAUST Solar Center Competitive Fund (CCF) for financial support. GIWAXS/R-SoXS measurements and analysis by L. Ye and H. Ade are supported by ONR grant N00141512322 and KAUST's Center Partnership Fund (No. 3321). X-ray data were acquired at beamlines 7.3.3 and 11.0.1.2 at the Advanced Light Source (ALS) in Berkeley National Lab, which is supported by the U.S. Department of Energy (DE-AC02-05CH11231). Z. Peng, S. Stuard, and I. Angunawela assisted with part of the R-SoXS data acquisition. C. Wang, C. Zhu, A.L.D. Kilcoyne, and E. Schaible are acknowledged for the beamline support. The material (IEICO-4F) was synthesized by H. Yao and J. Hou, which is supported by natural science foundation of china (21325419, 51373181 and 91333204).

Supporting Information Available.

Fabrication and Characterization of OSCs, J-Vs characteristics and photovoltaic parameters, optoelectronical measurements conditions and data, GIWAXS, RSoXS characterizations details and data, AFM images, absorption, photoluminescence and ellipsometry curves. List of recent works about current density, optical bandgap and device performance in solution-processable solar cells.

References:

(1) Yu, G.; Gao, J.; Hummelen, J. C.; Wudl, F.; Heeger, A. J. Polymer Photovoltaic Cells:

Enhanced Efficiencies via a Network of Internal Donor-Acceptor Heterojunctions. *Science.* **1995**, *270*, 1789–1791.

(2) Lu, L.; Zheng, T.; Wu, Q.; Schneider, A. M.; Zhao, D.; Yu, L. Recent Advances in Bulk Heterojunction Polymer Solar Cells. *Chem. Rev.* **2015**, *115*, 12666–12731.

(3) Ameri, T.; Li, N.; Brabec, C. J. Highly Efficient Organic Tandem Solar Cells: A Follow up Review. *Energy Environ. Sci.* **2013**, *6*, 2390.

(4) Lin, Y.; Zhan, X. Non-Fullerene Acceptors for Organic Photovoltaics: An Emerging Horizon. *Mater. Horizons* **2014**, *1* (5), 470-488.

(5) Cheng, Y. J.; Yang, S. H.; Hsu, C. S. Synthesis of Conjugated Polymers for Organic Solar Cell Applications. *Chem. Rev.* **2009**, *109*, 5868–5923.

(6) Günes, S.; Neugebauer, H.; Sariciftci, N. S. Conjugated Polymer-Based Organic Solar Cells. *Chem. Rev.* **2007**, *107*, 1324–1338.

(7) Liu, Y.; Zhao, J.; Li, Z.; Mu, C.; Ma, W.; Hu, H.; Jiang, K.; Lin, H.; Ade, H.; Yan, H. Aggregation and Morphology Control Enables Multiple Cases of High-Efficiency Polymer Solar Cells. *Nat. Commun.* **2014**, *5*, 5293.

(8) Lin, Y.; Zhan, X. Oligomer Molecules for Efficient Organic Photovoltaics. *Acc. Chem. Res.* **2016**, *49*, 175–183.

(9) Li, W.; Hendriks, K. H.; Furlan, A.; Roelofs, W. S. C.; Wienk, M. M.; Janssen, R. A. J. Universal Correlation between Fibril Width and Quantum Efficiency in Diketopyrrolopyrrole-Based Polymer Solar Cells. *J. Am. Chem. Soc.* **2013**, *135*, 18942–18948.

(10) Li, W.; Hendriks, K. H.; Furlan, A.; Wienk, M. M.; Janssen, R. A. J. High Quantum Efficiencies in Polymer Solar Cells at Energy Losses below 0.6 eV. *J. Am. Chem. Soc.*

2015, *137*, 2231–2234.

(11) Li, W.; Hendriks, K. H.; Wienk, M. M.; Janssen, R. A. J. Diketopyrrolopyrrole Polymers for Organic Solar Cells. *Acc. Chem. Res.* **2016**, *49*, 78–85.

(12) Baran, D.; Ashraf, R. S.; Hanifi, D. A.; Abdelsamie, M.; Gasparini, N.; Röhr, J. A.; Holliday, S.; Wadsworth, A.; Lockett, S.; Neophytou, M.; *et al* Reducing the Efficiency-Stability-Cost Gap of Organic Photovoltaics with Highly Efficient and Stable Small Molecule Acceptor Ternary Solar Cells. *Nat. Mater.* **2017**, *16*, 363–369.

(13) Nielsen, C. B.; Holliday, S.; Chen, H.-Y.; Cryer, S. J.; McCulloch, I. Non-Fullerene Electron Acceptors for Use in Organic Solar Cells. *Acc. Chem. Res.* **2015**, *48*, 2803–2812.

(14) Liu, F.; Zhou, Z.; Zhang, C.; Zhang, J.; Hu, Q.; Vergote, T.; Liu, F.; Russell, T. P.; Zhu, X. Efficient Semitransparent Solar Cells with High NIR Responsiveness Enabled by a Small-Bandgap Electron Acceptor. *Adv. Mater.* **2017**, *29*, 1606574.

(15) Wadsworth, A.; Ashraf, R. S.; Abdelsamie, M.; Pont, S.; Little, M.; Moser, M.; Hamid, Z.; Neophytou, M.; Zhang, W.; Amassian, A. *et al*. Highly Efficient and Reproducible Nonfullerene Solar Cells from Hydrocarbon Solvents. *ACS Energy Lett.* **2017**, *2*, 1494–1500.

(16) Song, X.; Gasparini, N.; Baran, D. The Influence of Solvent Additive on Polymer Solar Cells Employing Fullerene and Non-Fullerene Acceptors. *Adv. Electron. Mater.* **2017**, *2*, 1700358.

(17) Lin, Y.; Wang, J.; Zhang, Z.-G.; Bai, H.; Li, Y.; Zhu, D.; Zhan, X. An Electron Acceptor Challenging Fullerenes for Efficient Polymer Solar Cells. *Adv. Mater.* **2015**, *27*, 1170–1174.

(18) Zhao, W.; Li, S.; Yao, H.; Zhang, S.; Zhang, Y.; Yang, B.; Hou, J. Molecular

Optimization Enables over 13% Efficiency in Organic Solar Cells. *J. Am. Chem. Soc.* **2017**, *139*, 7148–7151.

(19) Cui, Y.; Yao, H.; Gao, B.; Qin, Y.; Zhang, S.; Yang, B.; He, C.; Xu, B.; Hou, J. Fine-Tuned Photoactive and Interconnection Layers for Achieving over 13% Efficiency in a Fullerene-Free Tandem Organic Solar Cell. *J. Am. Chem. Soc.* **2017**, *139*, 7302–7309.

(20) Yao, H.; Cui, Y.; Yu, R.; Gao, B.; Zhang, H.; Hou, J. Design, Synthesis, and Photovoltaic Characterization of a Small Molecular Acceptor with an Ultra-Narrow Band Gap. *Angew. Chemie Int. Ed.* **2017**, *56*, 3045–3049.

(21) Shi, X.; Zuo, L.; Jo, S. B.; Gao, K.; Lin, F.; Liu, F.; Jen, A. K.-Y. Design of a Highly Crystalline Low-Band Gap Fused-Ring Electron Acceptor for High-Efficiency Solar Cells with Low Energy Loss. *Chem. Mater.* **2017**, *29*, 8369–8376.

(22) Shockley, W.; Queisser, H. J. Detailed Balance Limit of Efficiency of P-n Junction Solar Cells. *J. Appl. Phys.* **1961**, *32*, 510–519.

(23) Tuladhar, S. M.; Azzouzi, M.; Delval, F.; Yao, J.; Guilbert, A. A. Y.; Kirchartz, T.; Montcada, N. F.; Dominguez, R.; Langa, F.; Palomares, E. *et al* Low Open-Circuit Voltage Loss in Solution-Processed Small-Molecule Organic Solar Cells. *ACS Energy Lett.* **2016**, *1*, 302–308.

(24) Zonno, I.; Martinez-Otero, A.; Hebig, J. C.; Kirchartz, T. Understanding Mott-Schottky Measurements under Illumination in Organic Bulk Heterojunction Solar Cells. *Phys. Rev. Applied*. **2017**, *7*, 034018.

(25) Yang, D.; Sasabe, H.; Sano, T.; Kido, J. Low-Band-Gap Small Molecule for Efficient Organic Solar Cells with a Low Energy Loss below 0.6 eV and a High Open-Circuit Voltage of over 0.9 V. *ACS Energy Lett.* **2017**, *2*, 2021–2025.

(26) Baran, D.; Kirchartz, T.; Wheeler, S.; Dimitrov, S.; Abdelsamie, M.; Gorman, J.; Ashraf, R. S.; Holliday, S.; Wadsworth, A.; Gasparini, N. *et al* Reduced Voltage Losses Yield 10% Efficient Fullerene Free Organic Solar Cells with >1 V Open Circuit Voltages. *Energy Environ. Sci.* **2016**, *9*, 3783–3793.

(27) Burkhard, G. F.; Hoke, E. T.; McGehee, M. D. Accounting for Interference, Scattering, and Electrode Absorption to Make Accurate Internal Quantum Efficiency Measurements in Organic and Other Thin Solar Cells. *Adv. Mater.* **2010**, *22*, 3293–3297.

(28) Bin, H.; Zhang, Z. G.; Gao, L.; Chen, S.; Zhong, L.; Xue, L.; Yang, C.; Li, Y. Non-Fullerene Polymer Solar Cells Based on Alkylthio and Fluorine Substituted 2D-Conjugated Polymers Reach 9.5% Efficiency. *J. Am. Chem. Soc.* **2016**, *138*, 4657–4664.

(29) Gasparini, N.; Jiao, X.; Heumueller, T.; Baran, D.; Matt, G. J.; Fladischer, S.; Spiecker, E.; Ade, H.; Brabec, C. J.; Ameri, T. Designing Ternary Blend Bulk Heterojunction Solar Cells with Reduced Carrier Recombination and a Fill Factor of 77%. *Nat. Energy* **2016**, *1*, 1–9.

(30) Stranks, S. D.; Stranks, S. D.; Eperon, G. E.; Grancini, G.; Menelaou, C.; Alcocer, M. J. P.; Leijtens, T.; Herz, L. M.; Petrozza, A.; Snaith, H. J. Electron-Hole Diffusion Lengths Exceeding. *Science* **2014**, *342*, 341–344.

(31) Song, X.; Wang, W.; Sun, P.; Ma, W.; Chen, Z.-K. Additive to Regulate the Perovskite Crystal Film Growth in Planar Heterojunction Solar Cells. *Appl. Phys. Lett.* **2015**, *106*, 33901.

(32) Zhang, J.; Zhang, Y.; Fang, J.; Lu, K.; Wang, Z.; Ma, W.; Wei, Z. Conjugated Polymer-Small Molecule Alloy Leads to High Efficient Ternary Organic Solar Cells. *J. Am. Chem. Soc.* **2015**, *137*, 8176–8183.

(33) Liu, S.; Song, X.; Thomas, S.; Kan, Z.; Cruciani, F.; Laquai, F.; Bredas, J.-L.; Beaujuge, P. M. Thieno[3,4- c]Pyrrole-4,6-Dione-Based Polymer Acceptors for High Open-Circuit Voltage All-Polymer Solar Cells. *Adv. Energy Mater.* **2017**, *7*, 1602574.

(34) Wan, J.; Xu, X.; Zhang, G.; Li, Y.; Feng, K.; Peng, Q. Highly Efficient Halogen-Free Solvent Processed Small-Molecule Organic Solar Cells Enabled by Material Design and Device Engineering. *Energy Environ. Sci.* **2017**, *10*, 1739–1745.

(35) Yang, L.; Zhang, S.; He, C.; Zhang, J.; Yao, H.; Yang, Y.; Zhang, Y.; Zhao, W.; Hou, J. New Wide Band Gap Donor for Efficient Fullerene-Free All-Small-Molecule Organic Solar Cells. *J. Am. Chem. Soc.* **2017**, *139*, 1958–1966.

(36) Lin, Y.; Zhao, F.; He, Q.; Huo, L.; Wu, Y.; Parker, T. C.; Ma, W.; Sun, Y.; Wang, C.; Zhu, D. *et al* High-Performance Electron Acceptor with Thienyl Side Chains for Organic Photovoltaics. *J. Am. Chem. Soc.* **2016**, *138*, 4955–4961.

(37) Hexemer, A.; Bras, W.; Glossinger, J.; Schaible, E.; Gann, E.; Kirian, R.; MacDowell, A.; Church, M.; Rude, B.; Padmore, H. A SAXS/WAXS/GISAXS Beamline with Multilayer Monochromator. *J. Phys. Conf. Ser.* **2010**, *247*.

(38) Gann, E.; Young, A. T.; Collins, B. A.; Yan, H.; Nasiatka, J.; Padmore, H. A.; Ade, H.; Hexemer, A.; Wang, C. Soft X-Ray Scattering Facility at the Advanced Light Source with Real-Time Data Processing and Analysis. *Rev. Sci. Instrum.* **2012**, *83* (4), 45110.

(39) Ye, L.; Jiao, X.; Zhou, M.; Zhang, S.; Yao, H.; Zhao, W.; Xia, A.; Ade, H.; Hou, J. Manipulating Aggregation and Molecular Orientation in All-Polymer Photovoltaic Cells. *Adv. Mater.* **2015**, *27* (39), 6046–6054.

(40) Tumbleston, J. R.; Collins, B. A.; Yang, L.; Stuart, A. C.; Gann, E.; Ma, W.; You, W.; Ade, H. The Influence of Molecular Orientation on Organic Bulk Heterojunction Solar

Cells. *Nat. Photonics* **2014**, *8*, 385–391.

(41) Jiao, X.; Ye, L.; Ade, H. Quantitative Morphology–Performance Correlations in Organic Solar Cells: Insights from Soft X-Ray Scattering. *Adv. Energy Mater.* **2017**, *7* , 1–22.

(42) Ye, L.; Xiong, Y.; Li, S.; Ghasemi, M.; Balar, N.; Turner, J.; Gadisa, A.; Hou, J.; O'Connor, B. T.; Ade, H. Precise Manipulation of Multilength Scale Morphology and Its Influence on Eco-Friendly Printed All-Polymer Solar Cells. *Adv. Funct. Mater.* **2017**, *27*, 1–10.

(43) Bauer, N.; Zhang, Q.; Zhao, J.; Ye, L.; Kim, J.-H.; Constantinou, I.; Yan, L.; So, F.; Ade, H.; Yan, H.; You, W. Comparing Non-Fullerene Acceptors with Fullerene in Polymer Solar Cells: A Case Study with FTAZ and PyCNTAZ. *J. Mater. Chem. A* **2017**, *5*, 4886–4893.

(44) Roland, S.; Schubert, M.; Collins, B. A.; Kurpiers, J.; Chen, Z.; Facchetti, A.; Ade, H.; Neher, D. Fullerene-Free Polymer Solar Cells with Highly Reduced Bimolecular Recombination and Field-Independent Charge Carrier Generation. *J. Phys. Chem. Lett.* **2014**, *5*, 2815–2822.

(45) Gasparini, N.; Salvador, M.; Strohm, S.; Heumueller, T.; Levchuk, I.; Wadsworth, A.; Bannock, J. H.; de Mello, J. C.; Egelhaaf, H.-J.; Baran, D.; McCulloch, I.; Brabec, C. J. Burn-in Free Nonfullerene-Based Organic Solar Cells. *Adv. Energy Mater.* **2017**, *7*, 1700770.

(46) Shuttle, C. G.; O'Regan, B.; Ballantyne, A. M.; Nelson, J.; Bradley, D. D. C.; de Mello, J.; Durrant, J. R. Experimental Determination of the Rate Law for Charge Carrier Decay in a Polythiophene: Fullerene Solar Cell. *Appl. Phys. Lett.* **2008**, *92*, 93311.

(47) Neher, D.; Kniepert, J.; Elimelech, A.; Koster, L. J. A. A New Figure of Merit for Organic

Solar Cells with Transport-Limited Photocurrents. *Sci. Rep.* **2016**, *6*, 24861.

(48) Mandoc, M. M.; Kooistra, F. B.; Hummelen, J. C.; de Boer, B.; Blom, P. W. M. Effect of Traps on the Performance of Bulk Heterojunction Organic Solar Cells. *Appl. Phys. Lett.* **2007**, *91*, 263505.

(49) Wang, C.; Zhang, W.; Meng, X.; Bergqvist, J.; Liu, X.; Genene, Z.; Xu, X.; Yartsev, A.; Inganäs, O.; Ma, W.; Wang, E.; Fahlman, M. Ternary Organic Solar Cells with Minimum Voltage Losses. *Adv. Energy Mater.* **2017**, *7*, 1–10.

(50) Bartesaghi, D.; Pe´rez, I. D. C.; Kniepert, J.; Roland, S.; Turbiez, M.; Neher, D.; Koster, L. J. A. Competition between Recombination and Extraction of Free Charges Determines the Fill Factor of Organic Solar Cells. *Nat. Commun.* **2015**, *6*, 8083.

(51) Holliday, S.; Ashraf, R. S.; Wadsworth, A.; Baran, D.; Yousaf, S. A.; Nielsen, C. B.; Tan, C.-H.; Dimitrov, S. D.; Shang, Z.; Gasparini, N.*et al*. High-Efficiency and Air-Stable P3HT-Based Polymer Solar Cells with a New Non-Fullerene Acceptor. *Nat. Commun.* **2016**, *7*, 11585.

(52) Mukherjee, S.; Jiao, X.; Ade, H. Charge Creation and Recombination in Multi-Length Scale Polymer:Fullerene BHJ Solar Cell Morphologies. *Adv. Energy Mater.* **2016**, *6*, 1–8.

(53) Mukherjee, S.; Proctor, C. M.; Tumbleston, J. R.; Bazan, G. C.; Nguyen, T. Q.; Ade, H. Importance of Domain Purity and Molecular Packing in Effi Cient Solution-Processed Small-Molecule Solar Cells. *Adv. Mater.* **2015**, *27*, 1105–1111.

(54) Huang, J.; Carpenter, J. H.; Li, C. Z.; Yu, J. S.; Ade, H.; Jen, A. K. Y. Highly Efficient Organic Solar Cells with Improved Vertical Donor-Acceptor Compositional Gradient Via an Inverted Off-Center Spinning Method. *Adv. Mater.* **2016**, *28*, 967–974.

Figures:

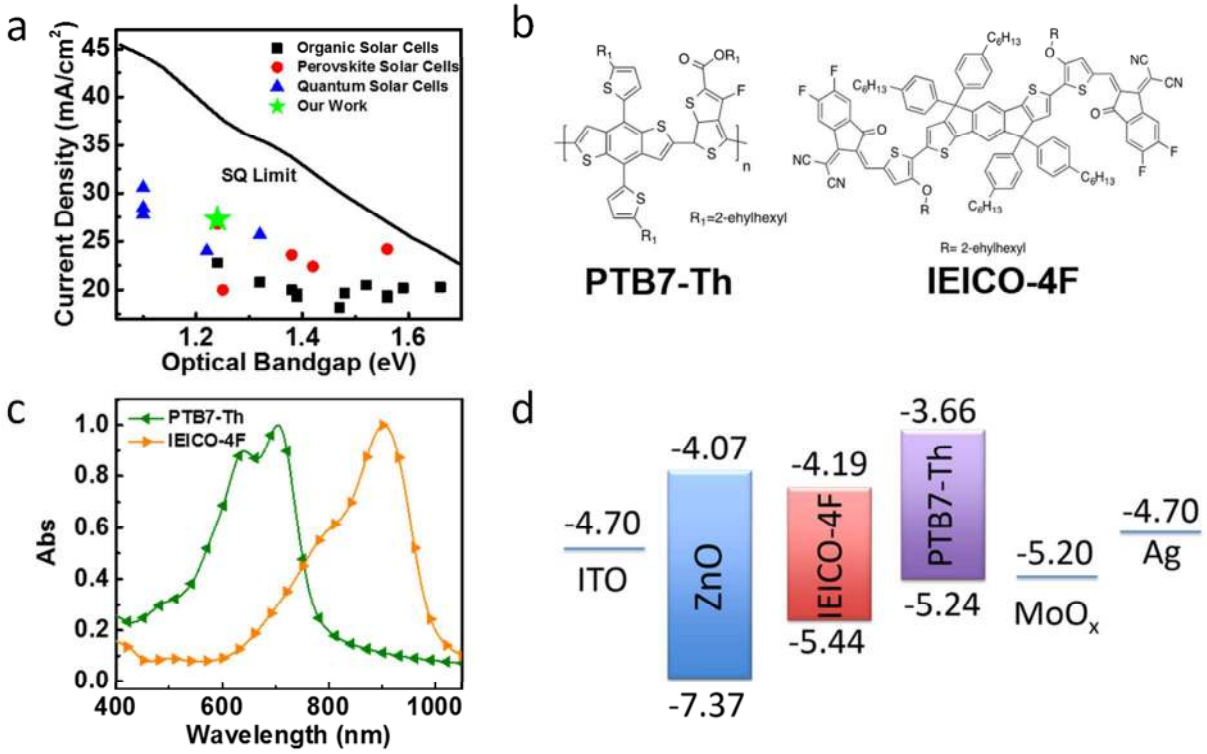

Figure 1. a) The map of bandgap vs Current Density with the lines of SQ limit; b) Chemical structures of PTB7-Th and IEICO-4F; c) Normalized thin film absorbance of PTB7-Th and IEICO-4F; d) the energy alignment of the materials used in the inverted solar cell.

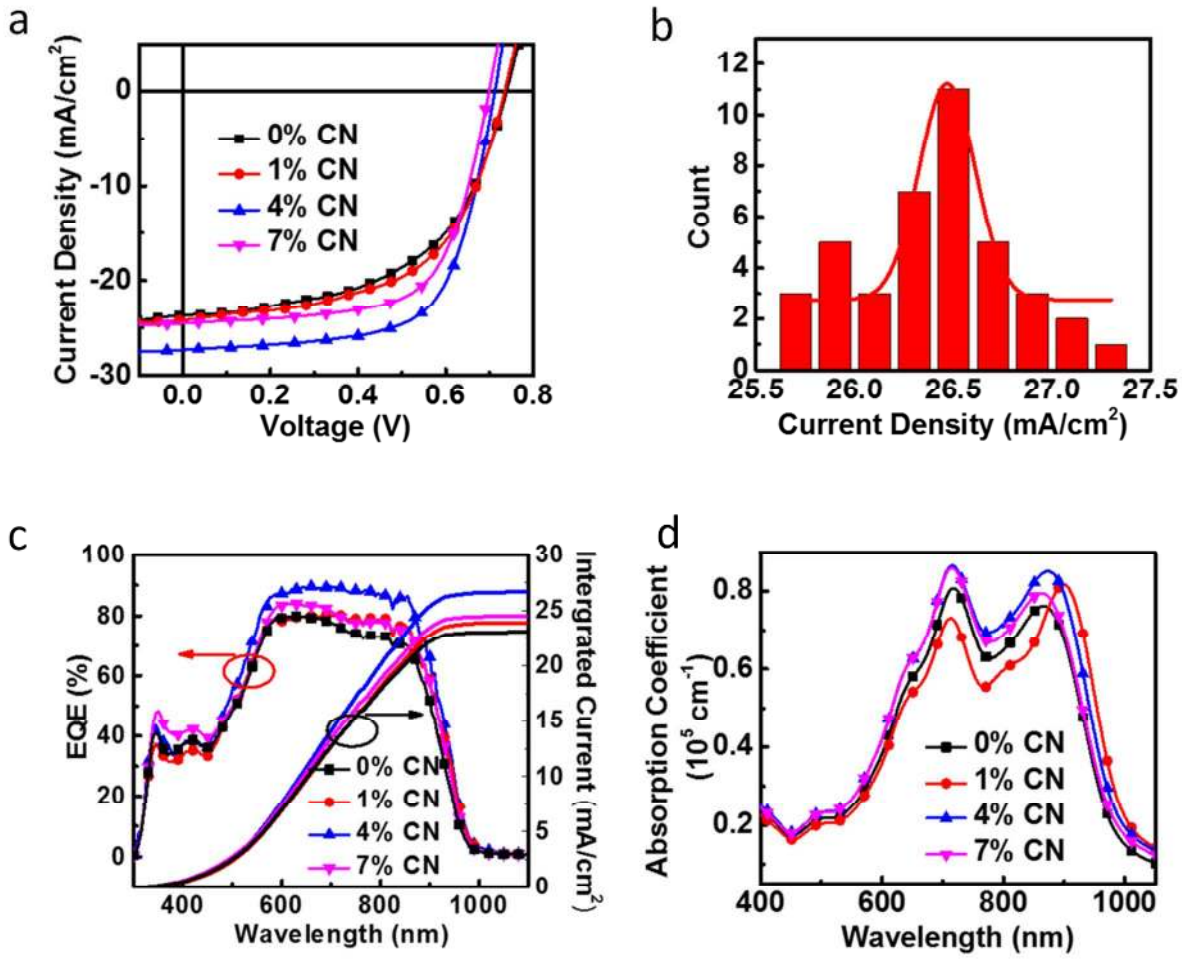

Figure 2. a) Current-Voltage characteristics (J-V) of PTB7-Th:IEICO-4F with different content of CN under 100 mWcm-2 light illumination; b) The current density distribution histogram; c) External quantum efficiency (EQE) (left side) and corresponding integrated current density of the devices (right side); d) Absorption coefficient spectra of thin films of PTB7-Th:IEICO-4F blends with different content of CN.

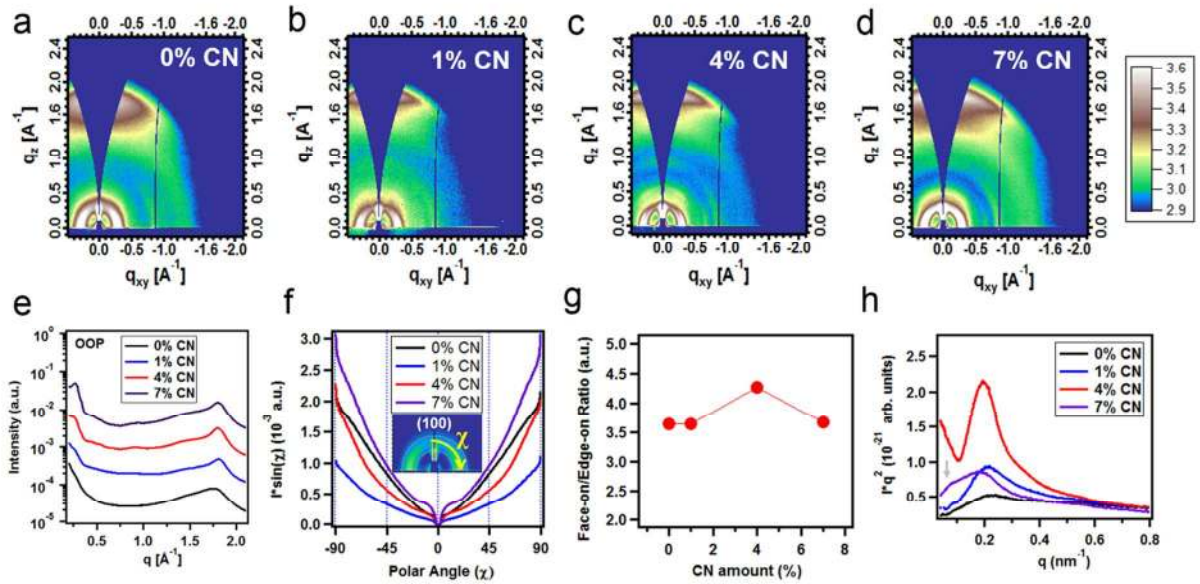

Figure 3. GIWAXS 2D patterns of PTB7-Th:IEICO-4F blend film with a) 0% CN, b) 1% CN, c) 4% CN and d) 7% CN respectively; e) GIWAXS out-of-plane (OOP) profiles of the blends with different amounts of CN; f) Corrected pole figure of (100) peaks of the blend films with different amounts of CN; g) Face-on-to edge-on ratio as a function of CN amount used; h) Lorentz corrected R-SoXS profiles of PTB7-Th:IEICO-4F blend films with different amount of CN.

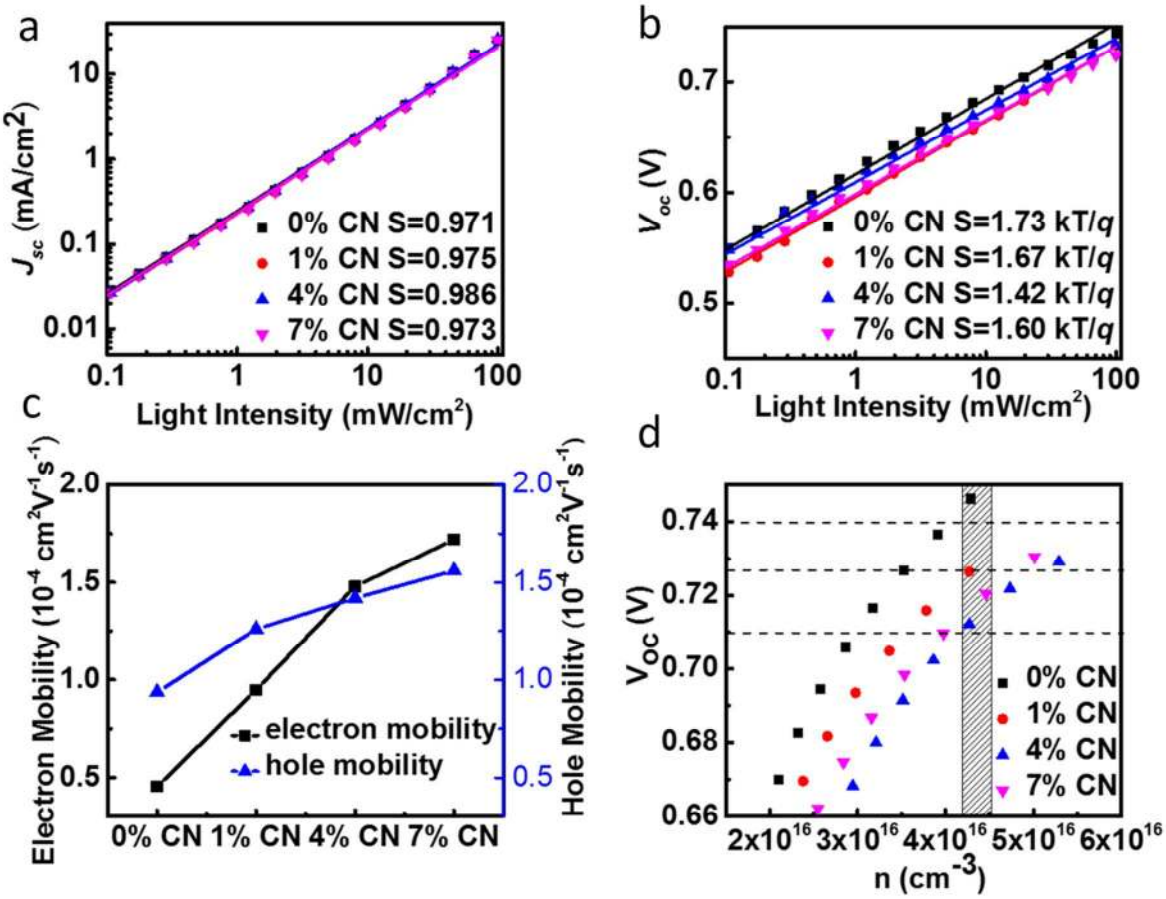

Figure 4. a,b) The J_{sc} and V_{oc} versus light intensity based on devices with different amount of CN; c) Comparison of hole and electron mobility of PTB7-Th:IEICO-4F blend film with 0% CN, 1% CN, 4% CN and 7% CN, respectively; d) Open-circuit voltage as a function of charge density of PTB7-Th:IEICO-4F blend film with 0% CN, 1% CN, 4% CN and 7% CN, respectively.

Table 1. Photovoltaic performances and hole, electron mobility of solar devices based on PTB7-Th:IEICO-4F blend film with 0% CN, 1% CN, 4% CN and 7% CN, respectively.

Blend Film	J_{sc} (mA/cm^2)	Integrated J_{sc} (mA/cm^2)	V_{oc} (mV)	FF (%)	PCE (%)	Ave PCE (%)[a]	μ_h (cm^{2}V^{-1}s^{-1})	μ_e (cm^{2}V^{-1}s^{-1})	μ_e/μ_h ratio	PTB7-Th PL Quenching (%)[b]
0% CN	23.7	23.1	736	53.6	9.41	9.23	9.35×10^{-5}	4.56×10^{-5}	0.49	87
1% CN	24.1	23.9	734	56.3	9.97	9.72	1.26×10^{-4}	9.47×10^{-5}	0.75	89
4% CN	27.3	26.8	712	65.7	12.8	12.1	1.42×10^{-4}	1.48×10^{-4}	1.04	96
7% CN	24.5	24.3	699	65.5	11.2	10.7	1.56×10^{-4}	1.72×10^{-4}	1.10	87

a): Power conversion efficiencies are averaged for 10 devices. b) The % PL quenching values are achieved by comparing blend PL to pristine PTB7-Th PL intensity.

Table 2. The GIWAXS and R-SoXS parameters of PTB7-Th:IEICO-4F blend films with 0% CN, 1% CN, 4% CN and 7% CN, respectively.

Blend Film	Peaks (Å^{-1}) Polymer, NFA	FWHM Polymer, NFA	OOP π-π Coherence Length (nm) Polymer, NFA	NFA intensity[a]	Long Period (nm)	ISI
0% CN	1.64, 1.78	0.48, 0.20	1.2, 2.8	0.71	30.1	0.50
1% CN	1.68, 1.81	0.48, 0.14	1.2, 4.0	0.62	30.0	0.63
4% CN	1.66, 1.80	0.54, 0.14	1.1, 4.0	1.00	31.4	1.00
7% CN	1.66, 1.81	0.51, 0.14	1.1, 4.0	0.90	33.0	0.59

a): Intensities are defined as the volume normalized peak area of OOP π-π stacking peak of NFAs and the highest intensity of 4% CN sample is set as 1.